OPTOELECTRONICS AND ADVANCED MATERIALS – RAPID COMMUNICATIONS Vol. 7, No. 11-12, November - December 2013, p. 1015-1020

Fabrication and characterization of metal to insulator phase transition thin films

HUIQUN ZHU[a,b], YI LI[a,c*], GUOXIANG TONG[a], BAOYING FANG[a], XIAOHUA WANG[a]
[a]*College of Optical-Electrical and Computer Engineering, University of Shanghai for Science and Technology, Shanghai 200093, People's Republic of China*
[b]*College of Applied Physics and Materials, Wuyi University, Jiangmen 529020, People's Republic of China*
[c]*Shanghai Key Laboratory of Modern Optical System, Shanghai 200093, People's Republic of China*

VO_2 thin films were successfully fabricated on glass substrates by magnetron sputtering at room temperature and thermal oxidation in the air. The structures, compositions, and optical properties of the films were characterized. Raman scattering and X-ray photoelectron spectroscopy demonstrated that the films were mostly composed of VO_2. X-ray diffraction and scanning electron microscopy patterns showed the relation between crystal structures and thermal oxidation. The optical measurement results showed the infrared transmittance variation of the film was above 50 % at 2500 nm, and the width of the thermal-hysteresis loop of the film was about 8 ^oC. The VO_2 thin films presented a good characterization from metal to insulator phase transition.

(Received June 24, 2012; accepted November 7, 2013)

Keywords: Vanadium dioxide, Sputtering, Oxidation, Phase transition

---

1. Introduction

Vanadium dioxide (VO_2) is an attracted smart material [1, 2]. It has a metal to insulator phase transition (MIT) about 68 °C, where there is a structural change from higher temperature rutile structure to a lower temperature monoclinic structure [3]. The distortion in the crystal structure brings about abrupt changes in the optical and electrical properties of VO_2 [4]. The phase transition occurs quickly under ideal conditions, usually within 10^{-3}-10^{-12} s [5]. These characteristics provide a large potential to VO_2 such as smart window material [6, 7], infrared light switch and sensor [8, 9], and so on. However, the phase transition temperature of VO_2 is still higher than room temperature, and a low infrared transmittance variation of VO_2 will decline the efficiency of phase transition. These problems of VO_2 thin films even obstacle the application of photoelectric high-tech fields [10]. Therefore, fabrication and evaluation of high quality VO_2 thin films still need more investigation.

Many approaches have been explored to prepare VO_2 thin films, including chemical vapor deposition [11], pulsed laser deposition [12], sol-gel process [13], hydrothermal method [14], magnetron sputtering [9, 15], ion beam sputtering [16] and so on. Among these ways, sputtering method seems better, because it can provide safety, high deposition rate, good surface adhesion to different substrates, and be more likely to extending to large-scale substrates used in the practical applications.

In previous sputtering experiments [17, 18], VO_2 films prepared with high substrate temperature, oxygen atmosphere, and vacuum annealing method were well studied. Sapphire, quartz, silicon and some single crystal materials were widely used. In order to solve the problems of VO_2 thin films including high phase transition temperature, broad width of thermal hysteresis loop and lower infrared transmittance, in this paper, VO_2 thin films were prepared on the glass substrates by magnetron sputtering at room temperature, then the prepared metal thin films were sufficiently oxidized to the thermochromic thin films by annealing under the air condition. Then we discussed the effects of structures and compositions on MIT of the VO_2 films.

2. Experiments

2.1. Preparation of VO_2 films

The metal to insulator phase transition thin films were prepared on the glass substrates by direct current magnetron sputtering (JC500-3/D) combining thermal oxidation method, namely the two-step method.

The glass substrates were dipped in acetone, ethanol and de-ionized water respectively and clean with ultrasonic washer for five minutes. Then they were dried up by nitrogen blowing before loading into a sputtering chamber. The vacuum chamber was evacuated to less than 10^{-4} Pa before introducing argon gas (5N purity). Flow rate and pressure of the argon gas was 80 sccm and 0.4 Pa, respectively. The V-metal target (4N purity, 120 mm in diameter) was pre-sputtered for several minutes to remove surface contamination before depositing the films. During the period of V-metal film deposition, the sputtering chamber was kept at room temperature, without adding curing voltage to heat substrates.

The V-metal thin films were taken out from the chamber, placed in the resistance furnace (SX2-4-10) with a temperature accuracy of ±1 °C for further oxidation. Then the prepared metal thin films were sufficiently oxidized to the thermochromic thin films by annealing under the air condition.

2.2. Measurements

The molecular structure and components of VO_2 films were measured at temperatures ranging from 25 to 100 ^{o}C by UV-NIR confocal laser micro Raman spectrometer (LabRAM HR) using a laser diode emitting at 488 nm. The morphologies and the average thicknesses of the samples were determined by a thermal field emission scanning electron microscopy (SEM, Nova Nano SEM 430). The composition of the films was examined by an X-ray photoelectron spectroscopy (XPS, PHI-5000C ESCA). MgKα radiation was served as a photoelectron excitation source of XPS including 54° angle of incidence and sampling spot of 800 μm. The crystallographic phase was analyzed with an X-ray diffractometer (XRD, BD90) using $CuK\alpha_1$ radiation (λ=0.15405nm). The operation was in the θ-2θ scan mode, working current of 30 A, and voltage of 36 KV. Reflection and transmission spectra were examined by a spectrophotometer (Lambda 1050) to observe the optical properties in the visible and infrared bands.

3. Results and discussion

3.1 Morphologies

An SEM pattern of the V-metal film deposited by sputtering at room temperature is shown in Fig. 1, which inset is a cross-sectional SEM pattern. SEM shows the particles of the V-metal film rather uniformly distribute on the substrate. The sizes of particles are about 15 nm. The thickness of the V-metal film is about 300 nm.

To understand the relation between crystal structures and thermal oxidation, the V-metal film sample was cut into four small pieces with the same size. They were consequently oxidized to the thermochromic thin films with different temperature and time respectively.

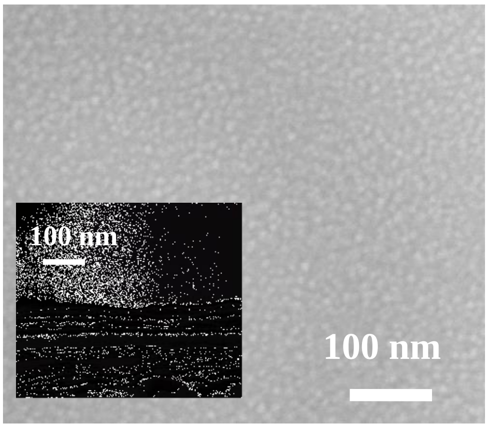

Fig. 1. The SEM pattern of the V-metal film deposited at room temperature.

Fig. 2 shows that four VO_2 film samples grown on glass substrates are quite different morphologies with the different oxidation conditions. In Figs. 2(a) and 2(b), the films both are distorted and nonuniform because of agglomeration of the crystalline grains. A possible explanation is the V-metal film does not have enough energy to absorb oxygen atoms to form a perfect surface through thermal oxidation at too low temperature, or for too short a time. As can be seen from Fig. 2(c), the film displayed a smooth and uniform surface without any distortion. There are smaller flake-like grains with about 60 nm in width and 200 nm in length on the substrate. In Fig. 2(d), the film shows a disorder crystalline flat-bar like structure. We notice that the grain size becomes obviously large and the film is not uniform. The SEM patterns show that oxidation temperature and time are important to the crystal size and the film morphologies.

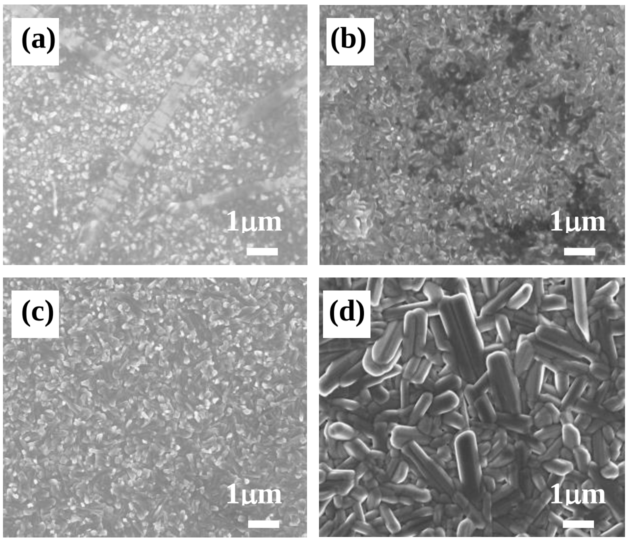

Fig. 2. SEM patterns of the VO_2 films oxidized at: (a) 360 °C for 4 h, (b) 380 °C for 2 h, (c) 380 °C for 4 h, (d) 400 °C for 4 h.

3.2 Crystallographic phase

X-ray diffraction patterns of the thin films are shown in Fig. 3. Three typical diffraction peaks at about 28°, 42°, and 55° can be characterized by VO_2 (011), VO_2 (210), and VO_2 (220) crystal planes, respectively [01-082-0661]. The thin films formed on the glass substrates present a polycrystalline VO_2 structure.

The crystallographic phase and intensity express different features with the different oxidation temperature and time. In Fig. 3a, there is one strong diffraction peak VO_2 (011) and some weakened peaks VO_2 (210), VO_2 (220), and VO_2 (102). When the oxidation temperature increases to 380 ° C (Fig. 3b), the intensity of VO_2 (011) peak enhances, and the others weaken. With oxidation time prolongs (Fig. 3c), the diffraction peak of VO_2 (102) disappears, the intensities of VO_2 (210) and VO_2 (220) decrease. The film presents a high orientation along the VO_2 (011). The strongest intensity of VO_2 (011) shows the component of VO_2 (011) is the highest of the diffraction peaks. As the oxidation temperature reaches up to 400 °C (Fig. 3d), the intensity of VO_2 (011) peak decreases, and those of VO_2 (210) and VO_2 (220) increase. The peaks of V_2O_5 (301), VO_2 (100), VO_2 (102), and VO_2 (300) appear. There are two ingredients coexisting of vanadium oxide in the film. It shows that during the synthesis process of V-O bond by oxygen absorption, the film formation with coexisting multi-ingredients is due to competition of various valence states of vanadium oxide at higher temperature. By analysis of peak intensity, the major component of the films is monoclinic VO_2.

Meanwhile, the full width at half maximum (FWHM) of VO_2 (011) peak gradually decrease with increasing of oxidation temperature and time. Then crystallite sizes belonged to VO_2 (011) are also gradually increased. Based on Scherrer equation, crystallite sizes corresponding to VO_2 (011) plane of the samples are calculated as shown in Table 1. The XRD results show that oxidation temperature and time have significantly changed the orientation, purity, and crystallite size of the thin films. These could affect the MIT of the vanadium oxide films.

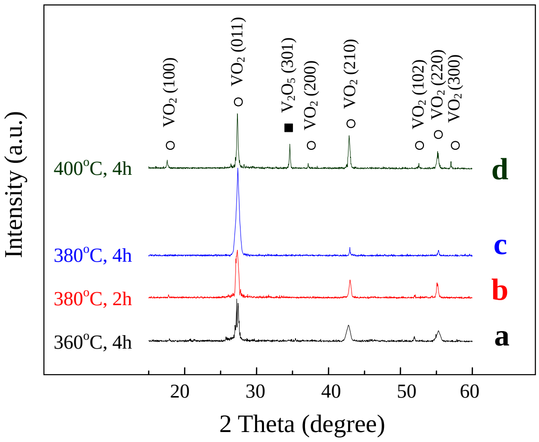

Fig. 3. XRD spectra of the VO_2 films oxidized on different conditions.

3.3 Raman spectra

Fig. 4 shows the Raman spectra of the samples oxidized at 360°C, 380°C, and 400°C for four hours. The curves were smoothed with a second order Savitzky–Golay function. We can see the presence of VO_2 with typical Raman peaks near 148, 192, 223, 269, 326, 395, 443, 515 and 616 cm^{-1} [6, 19]. The strong peaks of three samples are at 148, 269, 515 and 616 cm^{-1}, while the peaks at 192, 223, 326, 395 and 443 cm^{-1} are weak. The strongest peak at 269 cm^{-1} of the sample could be due to the lattice bending vibrational modes of a bridge bond V^{4+}-O-V^{4+} vibration [20, 21]. The results show the VO_2 phase structures are predominant in the films [22, 23].

Since the relative structure and component of VO_2 vary in each case because of different oxidation temperature during growth, the intensities of the modes are different [21]. In Fig. 4, there are only five Raman-active vibrational modes of the sample. Three characteristic peaks near 192, 395 and 616 cm^{-1} are almost completely disappearing. It implies the structural units of VO_2 are far perfect, and the component of VO_2 is low. When oxidation temperature is 380 °C, Raman modes of the sample are in good agreement with the Database of Raman Spectroscopy (http://rruff.info) and literature values [24, 25]. The amplitude of the A_g-modes at 148, 269, and 443 cm^{-1} of the sample are stronger significantly compared to the other samples. Three important peaks of VO_2 at 192, 395 and 616 cm^{-1} appear significant, and the vibrational mode of 616 cm^{-1} reacts rather strongly. It suggests that the relevant structural units of VO_2 in the sample have greater mass and higher purity. After oxidation temperature reaching up to 400 °C, the vibrational mode near 289 cm^{-1} corresponding to V^{5+} are clearly observed, but three peaks of 192, 395 and 616 cm^{-1} appear hardly ever. This suggests the formation of V_2O_5 gradually increases and the component of VO_2 in the sample decreases simultaneously. XRD and Raman show a consensus of analytical results, that a suitable oxidation condition is the key to fabricate high purity VO_2 films.

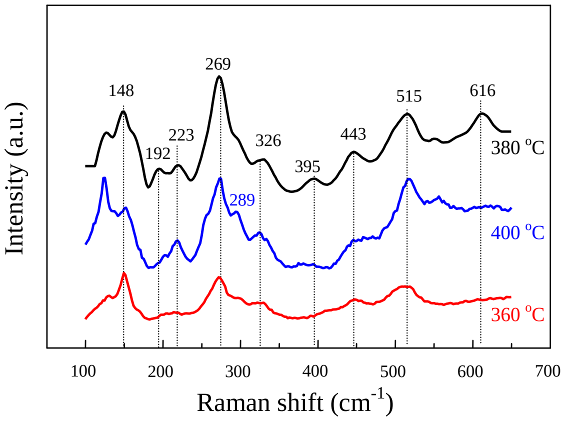

Fig. 4. Raman spectra of the VO_2 thin films oxidized at different temperature.

3.4. XPS spectroscopy

XPS is also used to explain the oxidation states of the V ions of the samples. Fig. 5 shows the XPS analysis of the sample prepared under the optimal oxidation condition. Fig. 5a shows V2p and O1s photoelectron spectra of the VO_2 film. According to the standard binding energy, the peaks at 516.83 and 523.25 eV, corresponding to $V2p_{3/2}$ and $V2p_{1/2}$, are due to the orbit splitting respectively [26]. The binding energy of 516.83 eV is between that of V^{4+} $2p_{3/2}$ and V^{5+} $2p_{3/2}$, and closes that of V^{4+} $2p_{3/2}$ [NIST XPS database]. It signals that the valence of V ions in the VO_2 thin films presents mainly as V^{4+}, a little amount of other vanadium oxide. To further determine the components and proportions of vanadium oxides in the film, we use the Xpspeak41 Software to fit $V2P_{3/2}$ peak cures of the sample as shown in Fig. 5b. It marks the curves of fitting of 515.64 and 517.20 eV correspond to V^{4+} and V^{5+} ions, with the proportion of 98.45% and 1.55%, respectively. XPS results demonstrate the samples are mainly consisted of VO_2 with a bit amount of V_2O_5.

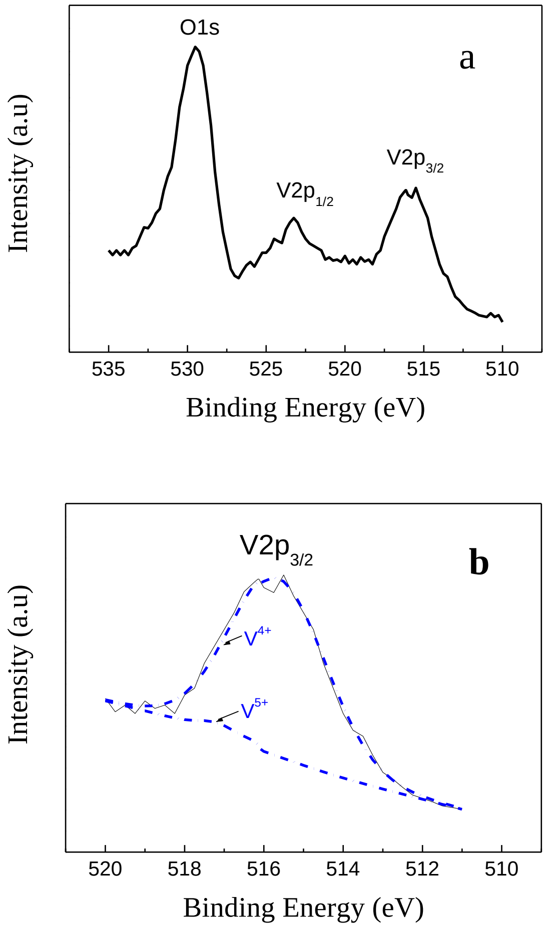

Fig. 5. XPS spectra of the VO_2 thin film.

3.5. Optical characterization

To research the relation between the structure and MIT characteristics of the VO_2 films, transmittance-wavelength curve, and reflectance-wavelength curve of VO_2 films were measured at 20 and 80 °C, respectively (Fig. 6). It is showed that the transmittance value at 20 °C (T_L) is always much higher than that at 80 °C (T_H). On the contrary, the reflectance value at 20 °C (R_L) is much lower than that at 80 °C (R_H), suggesting that an evident phase transition exists between 20 °C and 80 °C. The transmittance variation ($\Delta T = T_L - T_H$) increasing significantly in the infrared wavelength region behaves an optical switching characteristics of the samples. A plot of the thermal-hysteresis loop in the inset of Fig. 6 is a transmittance-temperature curve at a wavelength of 2500 nm. The hysteresis width of the samples with is in the range of 8-15 °C. The phase transition temperature (t_c) of the films defined as the temperature at the midpoint of the thermal-hysteresis loop. It is obvious that the phase transition temperature of the films is reduced more than 10 °C comparing with bulk material. The measurement results of the VO_2 thin films were summarized in Fig. 6 and Table 1.

It can be seen that transmittance variation and thermal-hysteresis loop width are quite different in the four samples. Figs. 6a and 6b show the ΔT are rather lower and the thermal-hysteresis loops are flat and wide. It implies that samples are oxidized insufficiently and crystallized imperfectly at low oxidation temperature or short oxidation time, leading to V^{4+}-V^{4+} bond imperfection, V^{4+} ions less and ΔT decline synchronously. As well as, many defects in the film result in strong absorption and diffuse scattering of photons leads to ΔT small, thermal-hysteresis loop flat and wide. In Fig. 6c, MIT of the sample is the best comparing with other VO_2 films. A steeper thermal-hysteresis loop of 8 ^{o}C and a larger ΔT of 52% at 2500nm are because of higher VO_2 component, better crystal orientation, and nanometer grain size. The high quality nanocrystalline would reduce both the related strain energy and IR diffuse scattering, which could result in a larger ΔT [27, 28]. On the other hand, the lower heat energy needed for small boundary of smaller grain to transfer the phase transition, leading to a narrow width of the thermal-hysteresis loop. When the sample oxidized at 400^{o}C (Fig. 6d), the MIT of the sample is increasingly awkward. XRD and Raman show the samples would be even more prone to another phase vanadium oxides at a higher oxidation temperature resulting in the component of VO_2 decreases. As well as, the grain sizes of the sample become large under the higher oxidation temperature (Table 1). The coexistence of polycrystalline mixed phase of VO_2 and V_2O_5, and the loss of energy transfer between larger size crystalline grains result in a flat and wide thermal-hysteresis loop and a low ΔT. It shows that metal-insulator transition properties are in connection with component and structure of the thin films. To control precisely the parameters of deposition and oxidation has played an important role in making up a good metal-insulator transition thin films.

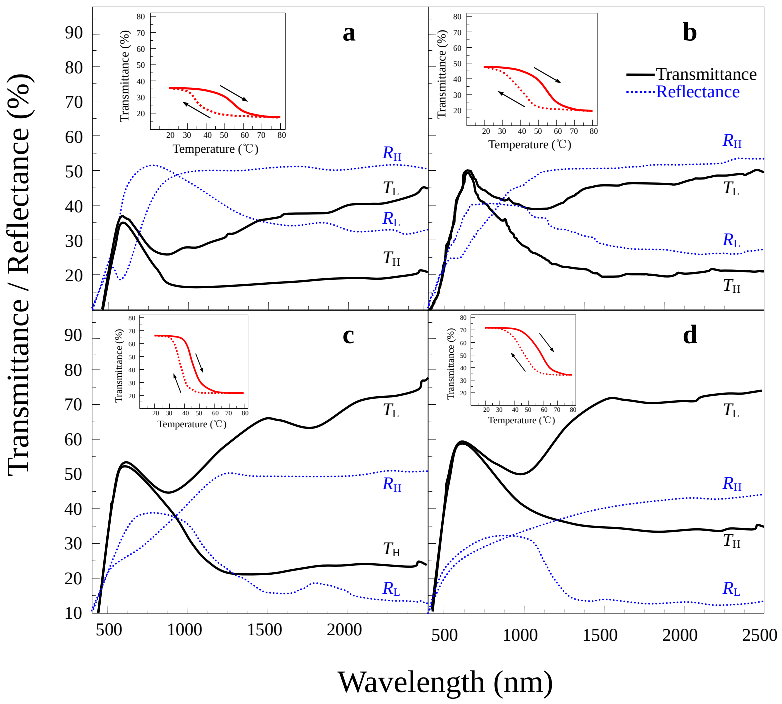

Fig. 6. Transmittance and reflectance spectra of the VO_2 films oxidized at: (a) 360 °C for 4 h, (b) 380 °C for 2 h, (c) 380 °C for 4 h, (d) 400 °C for 4h.

Table 1. Main grain sizes and properties of the samples under different oxidation conditions at wavelength of 2500 nm.

Sample	Oxidation condition	Main grain size / (nm)	T_L / (%)	T_H / (%)	ΔT / (%)	Hysteresis loop width / (°C)
a	360 °C, 4 h	41	45	21	24	15
b	380 °C, 2 h	43	49	21	28	13
c	380 °C, 4 h	45	76	24	52	8
d	400 °C, 4 h	51	74	35	39	10

4. Conclusion

In conclusion, the VO_2 thin films were prepared successfully on glass substrates by the two-step method that is sputtering V-metal films at room temperature then post thermal oxidation in the air. The results show the obtained films are nanoscale polycrystalline, high (011) oriented, and relative pure VO_2 contents. The infrared transmittance variation of the film is about 52% at 2500 nm. The width of the thermal-hysteresis loop of the film is about 8 °C. The significant metal-insulator transition of the VO_2 films on glass will stimulate the applications as intelligent materials.

Acknowledgments

This research was supported by the National High Technology Research and Development Program of China (No. 2006AA03Z348), the Innovation Fund Project for Graduate Student of Shanghai (No. JWCXSL1001), the Natural Scientific Foundation of Guangdong Province (No. 10152902001000025), the Science and Technology Program of Jiangmen City (No. JCG[2012]156), and the Shanghai Leading Academic Discipline Project (No. S30502).

References

[1] J. Du, Y. Gao, H. Luo, Sol. Energ. Mat. Sol. C., **95**, 1604 (2011).

[2] S. Ji, Y. Zhao, F. Zhang, J. Cryst. Growth, **312**, 282 (2010).

[3] M. Saeli, R. Binions, C. Piccirillo, Appl. Surf. Sci. **255**, 7291 (2009).

[4] Y. J. Cui, X. W. Wang, Y. Zhou, J. Cryst. Growth, **338**, 96 (2012).

[5] C. G. Granqvist, P. C. Lansaker, N. R. Mlyuka, Sol. Energ. Mat. Sol. C., **93**, 2032 (2009).

[6] S. H. Chen, J. J. Lai, J. Dai, Opt. Express **17**, 24153 (2009).

[7] F. B. Dejene, R.O. Ocaya, Curr. Appl. Phys., **10**, 508 (2010).

[8] B. G. Chae, H. T. Kim, Physica B: Condensed Matter **405**, 663 (2010).

[9] Y. Zhu, J. Na, F. He, Physica E, **52**,112 (2013).

[10] J. Nag, R. F. Haglund Jr, J. Phys.: Condens. Matter, **20**, 264016-1 (2008).

[11] R. Binions, G. Hyett, C. Piccirillo, J. Mater. Chem. **17**, 4652 (2007).

[12] J. Li, J. Dho n, J. Cryst. Growth, **312**, 3287 (2010).

[13] T. Chiub, K. Tonookaa, N. Kikuchia, Appl. Surf. Sci. **256**, 6834 (2010).

[14] K. C. Kam, A. K. Cheetham, Mater. Res. Bull. **41,** 1015 (2006).

[15] Y. Cui, X. Wang, Y. Zhou, J. Cryst. Growth, **338**, 96 (2012).

[16] B. Wang, S. Chen, Z. Huang, Appl. Surf. Sci. **258**, 5319 (2012).

[17] S. Saitzek, F. Guinneton, G. Guirleo, Thin Solid Films **516**, 891 (2008).

[18] Y. Nihei, Y. Sasakawa, K. Okimura, Thin Solid Films, **516**, 3572 (2008).

[19] E. U. Donev, R. Lopez, L. C. Feldman, R. F. Haglund, Jr., Nano Lett., **9,** 702 (2009).

[20] M. Pan, J. Liu, H. Zhong, S., J. Cryst. Growth **268**, 178 (2004).

[21] N. Rama, M. S. Ramachandra Rao, Solid State Comm. **150**, 1041 (2010).

[22] C. Juloen, G. A. Nazri, O. Bergstrom, Phys. Stat. Solidi B, **201**, 319 (1997).

[23] P. Schilbe, Physica B **316-317**, 600 (2002).

[24] A. G. Aronov, D. N. Mirlin, I. I. Reshina, Sov. Phys. Solid State **19,** 110 (1977).

[25] V. S. Vikhnin, I. N. Goncharuk, V. Y. Davydov, Phys. Solid State 37, 1971 (1995).

[26] J. Z. Yan, Y. Zhang, W. X. Huang, Thin Solid Films, **516**, 8554 (2008).

[27] Z. F Peng, Y. Wang, Y. Du, D. Lu, D. Sun, J. Alloys Compd. **48**, 537 (2009).

[28] J. C. Valmalette, J. R. Gavarri, Mater. Sci. Eng. B, **54,** 168 (1998).

---

*Corresponding author: optolyclp@263.net